Intermolecular interactions and the thermodynamic properties of supercritical fluids

Tesfaye M. Yigzawe and Richard J. Sadus[a)]
Centre for Molecular Simulation, Swinburne University of Technology, PO Box 218, Hawthorn, Victoria 3122, Australia

(Received 24 February 2013; accepted 19 April 2013; published online 16 May 2013)

The role of different contributions to intermolecular interactions on the thermodynamic properties of supercritical fluids is investigated. Molecular dynamics simulation results are reported for the energy, pressure, thermal pressure coefficient, thermal expansion coefficient, isothermal and adiabatic compressibilities, isobaric and isochoric heat capacities, Joule-Thomson coefficient, and speed of sound of fluids interacting via both the Lennard-Jones and Weeks-Chandler-Andersen potentials. These properties were obtained for a wide range of temperatures, pressures, and densities. For each thermodynamic property, an excess value is determined to distinguish between attraction and repulsion. It is found that the contributions of intermolecular interactions have varying effects depending on the thermodynamic property. The maxima exhibited by the isochoric and isobaric heat capacities, isothermal compressibilities, and thermal expansion coefficient are attributed to interactions in the Lennard-Jones well. Repulsion is required to obtain physically realistic speeds of sound and both repulsion and attraction are necessary to observe a Joule-Thomson inversion curve. Significantly, both maxima and minima are observed for the isobaric and isochoric heat capacities of the supercritical Lennard-Jones fluid. It is postulated that the loci of these maxima and minima converge to a common point via the same power law relationship as the phase coexistence curve with an exponent of $\beta = 0.32$. This provides an explanation for the terminal isobaric heat capacity maximum in supercritical fluids. © *2013 AIP Publishing LLC*. [http://dx.doi.org/10.1063/1.4803855]

I. INTRODUCTION

Thermodynamic properties have an important role in many biological, chemical, physical, and technical processes. Considerable emphasis has been placed on modelling and predicting thermodynamic properties using empirical correlations, statistical theories, and equations of state.[1,2] Molecular simulation[3] is a useful alternative to conventional theories because, when used properly, it provides unambiguous information regarding the merit of the underlying model. Increasingly, molecular simulation is being used to provide worthwhile predictions to both guide and supplement experimental work.

In general, the use of molecular simulation requires the *a priori* postulation of an intermolecular potential to evaluate inter-particle forces or energies. The Lennard-Jones (LJ) potential is arguably the most commonly used intermolecular potential because it incorporates the salient features of inter-particle interactions. For the LJ potential, the intermolecular energy (u) between particles i and j separated by a distance r_{ij} is obtained from

$$u(r_{ij}) = 4\varepsilon\left(\left(\frac{\sigma}{r_{ij}}\right)^{12} - \left(\frac{\sigma}{r_{ij}}\right)^{6}\right), \tag{1}$$

where ε and σ are the characteristic energy and distance parameters, respectively. Equation (1) represents the most commonly used "12-6" variant of the LJ potential whereas other choices of exponents are possible resulting in different observed behavior.[4] The LJ potential incorporates both attractive and repulsive interactions. Despite its relative simplicity, the LJ potential can reproduce the full range of fluid properties, including both solid-liquid[4] and vapor-liquid coexistence.[5] Although the LJ potential applies primarily to atomic systems or small molecules, it is also commonly used in the development of force fields[3] for macromolecules.

It has long been recognised[1] that the properties of fluids are often dominated by repulsive interactions and various separations of the contributions of inter-particle interactions have been suggested. McQuarrie and Katz[6] proposed a separation of the LJ potential based on the r^{-12} and r^{-6} terms. Barker and Henderson[7] separated the LJ potential based on regions that yield positive ($r_{ij} < \sigma$) and negative ($r_{ij} > \sigma$) values. Weeks *et al.*[8] identified purely repulsive and attractive contributions by splitting the LJ potential at a separation of $r_{ij} = 2^{1/6}\sigma$. The repulsive part of this separation is now commonly referred to as the Weeks-Chandler-Anderson (WCA) potential. It is the LJ potential truncated at the minimum potential energy at a distance $r_{ij} = 2^{1/6}\sigma$ on the length scale and shifted upwards by the amount ε on the energy scale such that both the energy and force are zero at or beyond the cut-off distance

$$u(r_{ij}) = \begin{cases} 4\varepsilon\left(\left(\frac{\sigma}{r_{ij}}\right)^{12} - \left(\frac{\sigma}{r_{ij}}\right)^{6}\right) + \varepsilon, & r_{ij} \le 2^{1/6}\sigma \\ 0 & r_{ij} > 2^{1/6}\sigma \end{cases}. \tag{2}$$

a)Email: rsadus@swin.edu.au

Equation (2) is a purely repulsive potential as such it can be only used for a limited range of properties. For example, it predicts solid-liquid equilibria but not vapor-liquid equilibria.

The LJ and WCA potentials have been widely investigated either as stand alone potentials or they have been incorporated as part of force fields for molecular systems.[9,10] In particular, the phase behavior of the LJ and WCA potentials is very well documented in the literature.[3,4,11] However, knowledge of the thermodynamic properties of the LJ and WCA potentials remains incomplete with available molecular simulation data largely confined[12] to quantities such as pressure (p), potential energy (U), isochoric (C_V) and isobaric (C_p) heat capacities. In contrast, other thermodynamic properties such as the thermal pressure coefficient (γ_v), thermal expansion coefficient (α_p), isothermal (β_T) and adiabatic (β_S) compressibilities, Joule-Thomson coefficient (μ_{jT}), and the speed of sound (w_0) are much less commonly reported.[13–16] Furthermore, simulations of thermodynamic properties in general are often confined to state points at ambient temperatures.

The relative lack of data can be partly attributed to the fact that only a few thermodynamic properties can be observed directly from conventional molecular simulations. The U, p, and temperature (T) are the only directly observable quantities available from microcanonical (NVE) ensemble simulations, which maintain a constant number of particles (N), volume (V), and total energy (E). This means that the calculation of other thermodynamic quantities requires the use of fluctuation formulas or equations of state.[17,18] Lustig[19–22] showed that, in principle, it is possible to calculate all thermodynamic state variables from key derivatives obtained directly from either molecular dynamics (MD) or Monte Carlo (MC) simulations. The method is based on the exact expressions for the thermodynamic state variables in the $NVE\vec{P}\vec{G}$ ensemble, which maintains both constant linear momentum ($\vec{P}$) and an additional quantity ($\vec{G}$) that is related to the initial position of the center of mass.

The advantage of the $NVE\vec{P}\vec{G}$ method is that it allows us to directly obtain all the thermodynamic quantities of a fluid from a single MD simulation. We will utilize this feature to comprehensively determine the full range of thermodynamic properties over a wide range of supercritical state points. By directly comparing the LJ and WCA results, our aim is to determine the role of different aspects of molecular interactions. The focus of this work is the near supercritical region in which fluids exhibit interesting behavior such as percolation transitions in water.[23] In particular, we investigate the occurrence of maxima and minima in thermodynamic properties in the supercritical phase.

II. MD SIMULATIONS

A. Overview of the $NVE\vec{P}\vec{G}$ method

The method has been discussed in detail in Refs. 19, 24, and 25 and only a brief outline of the salient features is given here. The fundamental equation of state for the system is defined by the entropy (S) postulate,[24] i.e.,

$$S(N, V, E, \vec{P}, \vec{G}) = k \ln \mathbf{\Omega}(N, V, E, \vec{P}, \vec{G}), \tag{3}$$

where $\mathbf{\Omega}(N, V, E, \vec{P}, \vec{G})$ is the phase-space volume and k is the Boltzmann constant. The basic phase-space functions are then introduced as an abbreviation representing the derivatives of the phase-space volume with respect to the independent thermodynamic state variables

$$\Omega_{m\,n} = \frac{1}{\omega}\frac{\partial^{m+n}\Omega}{\partial E^m \partial V^n}, \tag{4}$$

where ω is the phase-space density. The exact derivation of the phase-space function is quite involved and the full expression is given in Ref. 24. A feature of the determination of the Ω terms is the evaluation of volume derivatives of the potential energy

$$\frac{\partial^n U}{\partial V^n} = \frac{1}{3^n V^n}\sum_{i=1}^{N-1}\sum_{j=i+1}^{N}\sum_{k=1}^{n} a_{n\,k} r_{i\,j}^{k}\frac{\partial^k u}{\partial r_{i\,j}^{k}}, \tag{5}$$

where the coefficients $a_{n\,k}$ are constructed using a recursion relation. All thermodynamic state variables are then expressible in terms of the phase-space function. The resulting thermodynamic state variables used in this work are summarized in Table I. In effect, the $NVE\vec{P}\vec{G}$ ensemble simulations

TABLE I. Thermodynamic properties expressed in terms of phase-space functions.

Temperature	$T = \left(\frac{\partial E}{\partial S}\right)_V = \frac{\Omega_{00}}{k}$
Pressure	$p = T\left(\frac{\partial S}{\partial V}\right)_E = \Omega_{01}$
Isochoric heat capacity	$C_V = \left[\left(\frac{\partial^2 S}{\partial E^2}\right)_V\right]^{-1} = k\,(1 - \Omega_{00}\,\Omega_{20})^{-1}$
Thermal pressure coefficient	$\gamma_V = \left(\frac{\partial p}{\partial T}\right)_V = k\frac{\Omega_{11} - \Omega_{01}\,\Omega_{20}}{1 - \Omega_{00}\,\Omega_{20}}$
Isothermal compressibility	$\beta_T^{-1} = -V\left(\frac{\partial p}{\partial V}\right)_T = V\left[\frac{\Omega_{01}(2\Omega_{11} - \Omega_{01}\Omega_{20}) - \Omega_{00}\Omega_{11}^2}{1 - \Omega_{00}\Omega_{20}} - \Omega_{02}\right]$
Adiabatic compressibility	$\beta_S^{-1} = -V\left(\frac{\partial p}{\partial V}\right)_S = V\left[\Omega_{01}\,(2\Omega_{11} - \Omega_{01}\Omega_{20}) - \Omega_{02}\right]$
Speed of sound	$w_0^2 = -\frac{V^2}{M}\left(\frac{\partial p}{\partial V}\right)_S = \frac{V^2}{M}\left[\Omega_{01}\,(2\Omega_{11} - \Omega_{01}\Omega_{20}) - \Omega_{02}\right]$
Thermal expansion coefficient	$\alpha_P = \beta_T\ \gamma_V$
Isobaric heat capacity	$C_P = C_V\frac{\beta_T}{\beta_S}$
Joule-Thomson coefficient	$\mu_{J\,T} = V\frac{T\,\gamma_V\,\beta_T - 1}{C_P}$

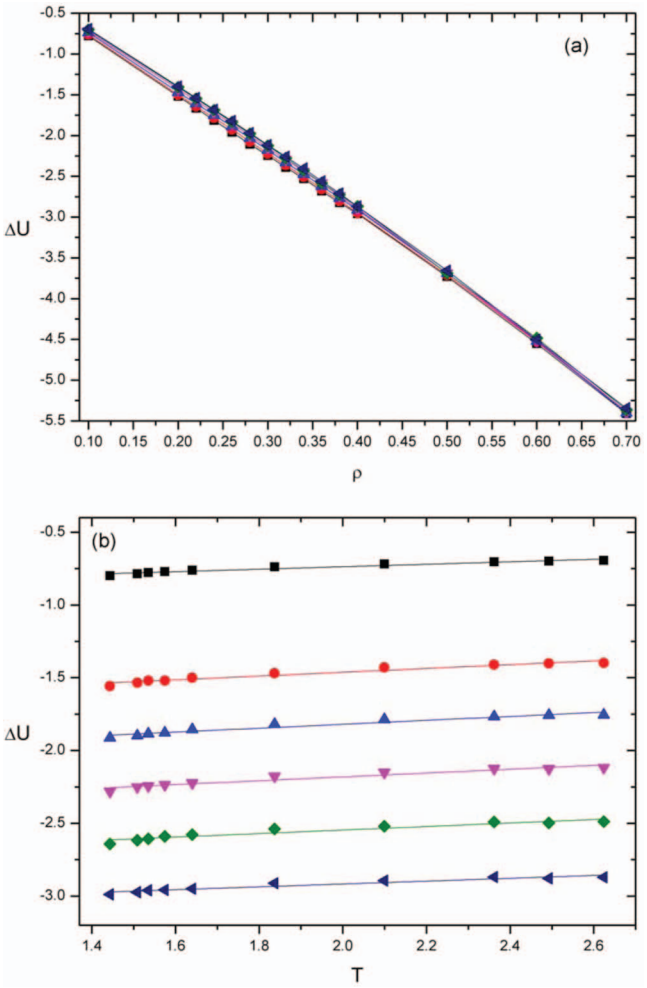

FIG. 1. ΔU as a function of (a) density at different temperatures corresponding to $\varphi = 1.17$ (black ■), 1.4 (blue ▲), 1.6 (pink ▼), 1.8 (green ◆), and 2.0 (dark blue ◄); and (b) temperature at different densities corresponding to $\rho = 0.1$ (black ■), 0.2 (red ●), 0.25 (blue ▲), 0.3 (pink ▼), 0.35 (green ◆), and 0.4 (dark blue ◄). The solid lines are for guidance only.

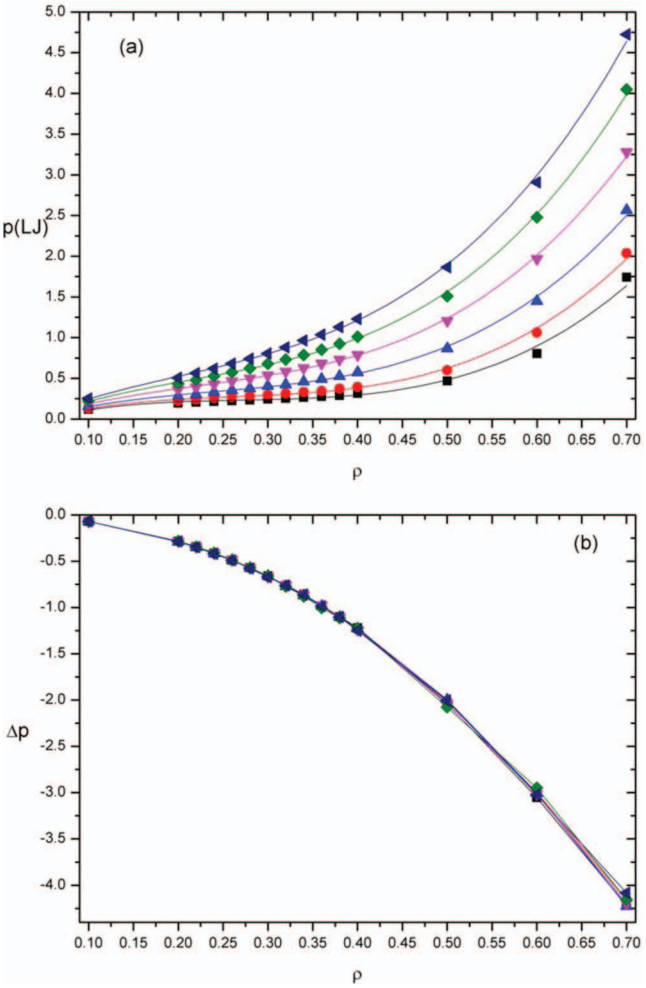

FIG. 2. (a) p for a LJ fluid and (b) Δp as a function of density at different constant temperatures corresponding to $\varphi = 1.17$ (black ■), 1.25 (red ●), 1.4 (blue ▲), 1.6 (pink ▼), 1.8 (green ◆), and 2.0 (dark blue ◄). The solid lines are for guidance only.

simply involve implementing a conventional $NVE\vec{P}$ simulation while keeping track of the volume derivatives of the intermolecular potential required for the evaluation of the thermodynamic quantities.

B. Simulation details

The $NVE\vec{P}\vec{G}$ MD simulations were performed for a homogenous fluid of 2000 particles interacting via the LJ and WCA potentials. The normal conventions were used for the reduced density ($\rho^* = \rho\sigma^3$), temperature ($T^* = kT/\varepsilon$), potential energy ($U^* = U/N\varepsilon$), pressure ($p^* = p\sigma^3/\varepsilon$), heat capacities ($C^*_{p,V} = C_{p,V}/k$), compressibilities ($\beta^*_{T,S} = \beta_{T,S}\ \varepsilon/\sigma^3$), thermal pressure coefficient ($\gamma^*_V = \gamma_V\ \sigma^3/k$), thermal expansion coefficient ($\alpha^*_P = \alpha_P\ \varepsilon/k$), speed of sound ($w^*_0 = w_0\sqrt{m/\varepsilon}$), where m is the mass of the particles, and the Joule-Thomson coefficient ($\mu^*_{J\ T} = \mu_{J\ T}\ k/\sigma^3$). All quantities quoted in this work are in terms of these reduced quantities and the asterisk superscript will be omitted in the rest of the paper.

The equations of motion were integrated using a five-value Gear predictor-corrector scheme[3,24] with a time step of 2 fs. For each state point, simulation trajectories were run for 6 or 10 × 10^6 time steps (12 or 20 ns) with 5 or 8 × 10^6 time steps (10 or 16 ns) used to equilibrate the WCA or LJ systems, respectively. For the LJ potential, the cut-off radius was $6.5\,\sigma$. Conventional long-range corrections[3] were used for U and p, whereas the long-range corrections for the volume derivatives were calculated from the formulas reported by Meier and Kabelac.[24] In Figs. 1–12, error bars are not shown because, in most cases, the calculated statistical uncertainties of the data points are similar to the size of the symbols.

III. RESULTS AND DISCUSSION

At all densities and temperatures, matching simulations were performed for both the LJ and WCA potentials to determine the thermodynamic properties. The ranges of temperatures and densities for our simulations were $1.312 \le T \le 2.624$ and $0.1 \le \rho \le 1.0$, respectively. It is convenient to represent temperatures as multiples of the reduced critical temperature of the LJ fluid,[27] $T_c = 1.312$. We denote these

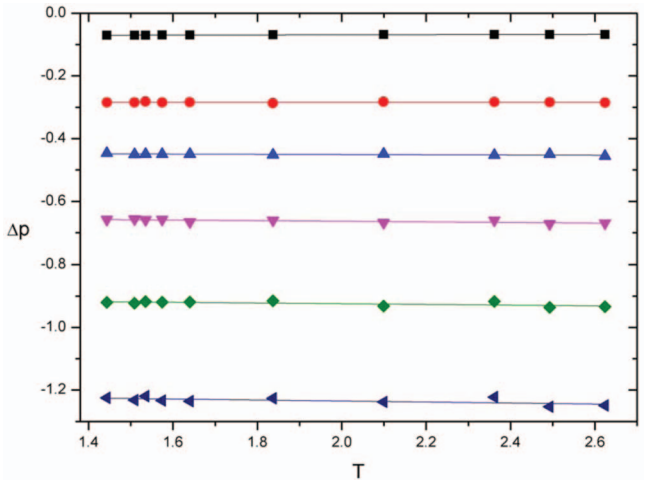

FIG. 3. Δp as a function of temperature at different constant densities corresponding to $\rho = 0.1$ (black ■), 0.2 (red ●), 0.25 (blue ▲), 0.3 (pink ▼), 0.35 (green ◆), and 0.4 (dark blue ◄). The solid lines are for guidance only.

multiples using the symbol $\varphi = T/T_c$, where, for example, $\varphi = 1.05$ means that $T = 1.05 \times T_c = 1.3776$. The simulations are reported at supercritical temperatures, which means that the fluid is in a single homogeneous phase at every possible density. In contrast, simulations at sub-critical temperatures would be limited to smaller discrete ranges of densities corresponding to either homogenous liquid or vapor phases. Finite size effects preclude the investigation of the critical point with the methods used here.

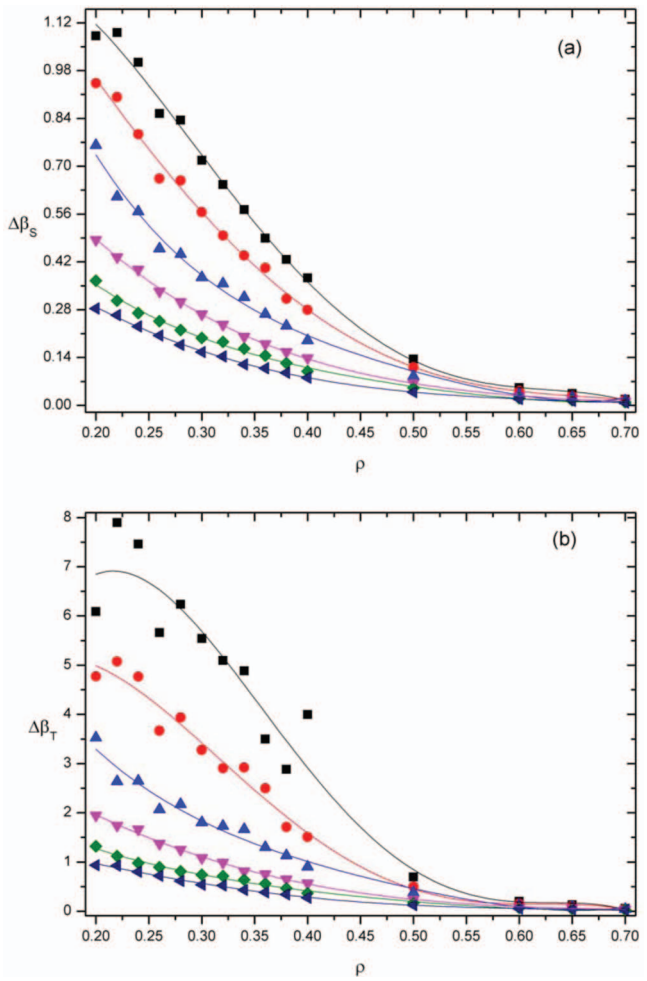

FIG. 4. (a) $\Delta\beta_S$ and (b) $\Delta\beta_T$ as a function of density at different constant temperatures corresponding to $\varphi = 1.17$ (black ■), 1.25 (red ●), 1.4 (blue ▲), 1.6 (pink ▼), 1.8 (green ◆), and 2.0 (dark blue ◄). The solid lines are for guidance only.

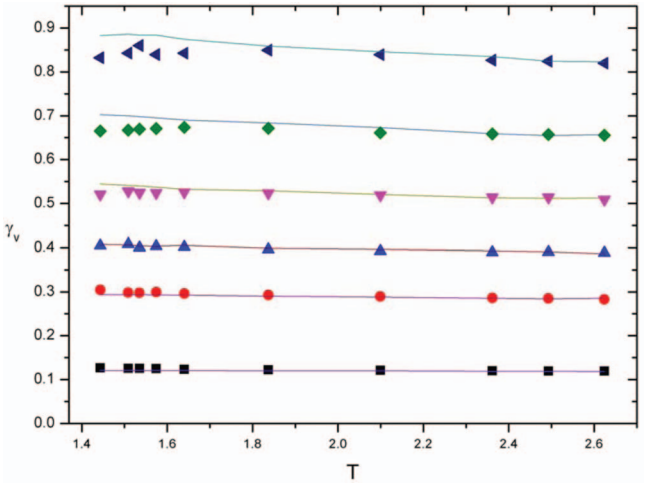

FIG. 5. γ_V as a function of temperature at different constant densities for the LJ (symbols) and WCA (solid lines) potentials. Results are shown for $\rho = 0.1$ (black ■), 0.2 (red ●), 0.25 (blue ▲), 0.3 (pink ▼), 0.35 (green ◆), and 0.4 (dark blue ◄). The solid lines are for guidance only.

In most cases, instead of illustrating the results separately, we have calculated the difference (Δ) between the LJ and WCA results, i.e.,

$$\left.\begin{aligned} \Delta U &= U_{LJ} - U_{WCA} \\ \Delta p &= p_{LJ} - p_{WCA} \\ \Delta\beta_{S,T} &= \beta_{S,T,LJ} - \beta_{S,T,WCA} \\ \Delta\alpha_p &= \alpha_{p,LJ} - \alpha_{p,WCA} \\ \Delta C_{p,V} &= C_{p,V,LJ} - C_{p,V,WCA} \\ \Delta\mu_{JT} &= \mu_{JT,LJ} - \mu_{JT,WCA} \\ \Delta w_0 &= w_{0,LJ} - w_{0,WCA} \end{aligned}\right\}. \quad (6)$$

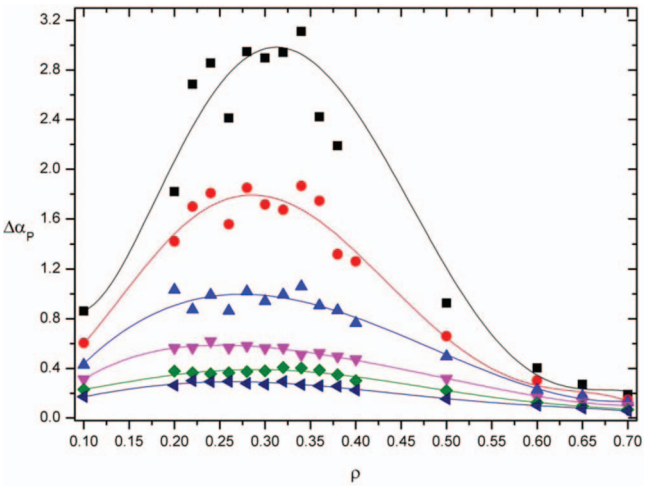

FIG. 6. $\Delta\alpha_p$ as a function of density at different constant temperatures corresponding to $\varphi = 1.17$ (black ■), 1.25 (red ●), 1.4 (blue ▲), 1.6 (pink ▼), 1.8 (green ◆), and 2.0 (dark blue ◄). The solid lines are for guidance only.

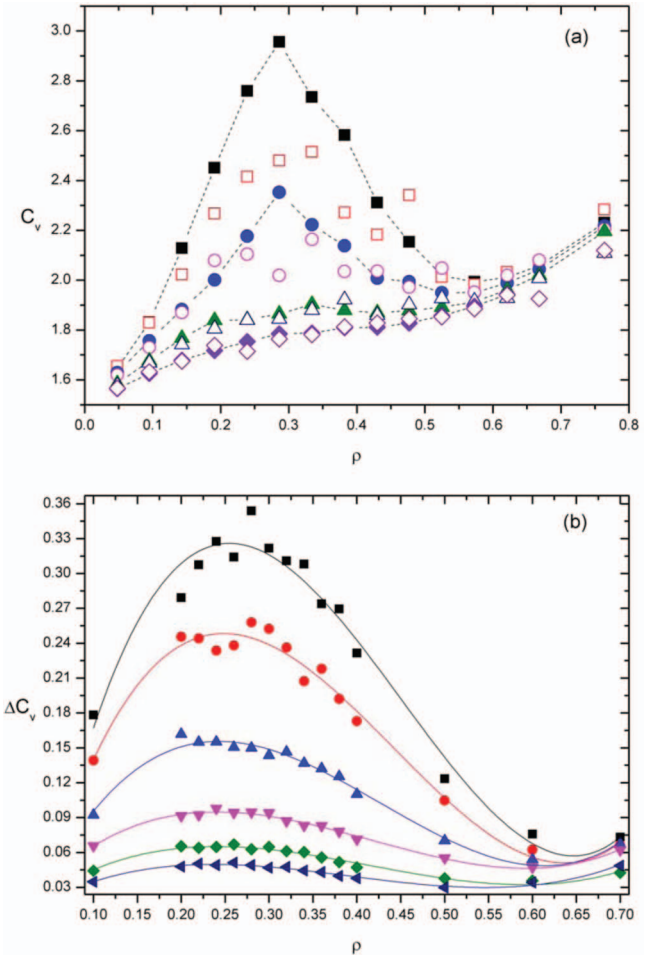

FIG. 7. (a) Comparison of LJ C_V values obtained in this work as a function of density at different constant temperatures of T = 1.3 (black ■), 1.4 (blue ●), 1.6 (green ▲), and 1.8 (purple ◆) with MC results reported by Freasier *et al.*[33] (identified by the corresponding open symbols); and (b) ΔC_V as a function of density at different constant temperatures corresponding to $\varphi = 1.17$ (black ■), 1.25 (red ●), 1.4 (blue ▲), 1.6 (pink ▼), 1.8 (green ◆), and 2.0 (dark blue ◄). The solid and dashed lines are for guidance only.

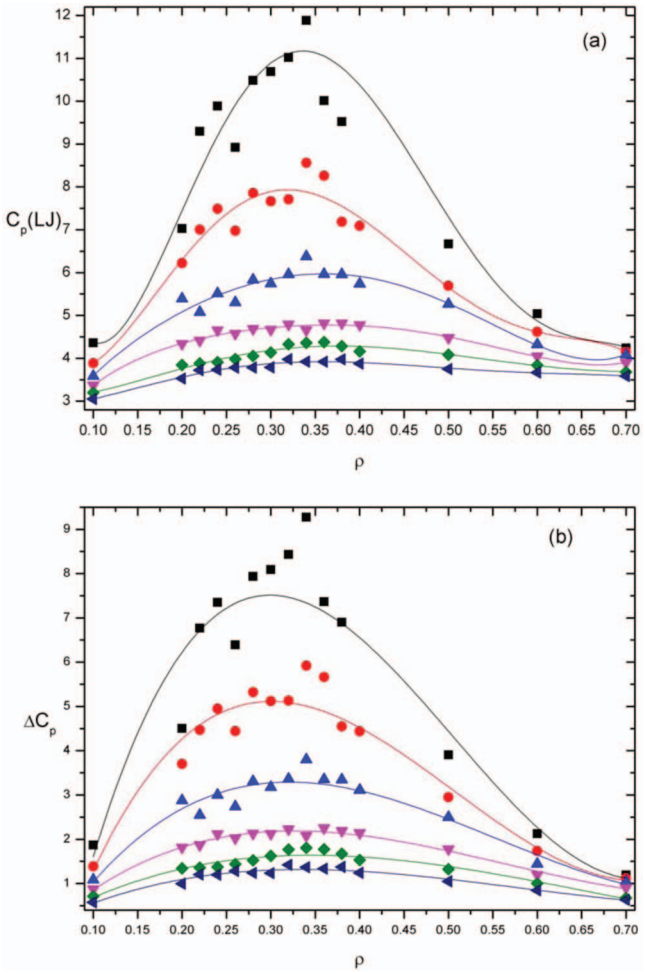

FIG. 8. (a) C_p for the LJ potential and (b) ΔC_p as a function of density at different constant temperatures corresponding to $\varphi = 1.17$ (black ■), 1.25 (red ●), 1.4 (blue ▲), 1.6 (pink ▼), 1.8 (green ◆), and 2.0 (dark blue ◄). The solid lines are for guidance only.

In effect, these difference values represent "excess" properties relative to the WCA potential. The kinetic or ideal gas term, common to both LJ and WCA simulations, is eliminated by the definition of these excess terms. The values obtained from Eq. (6) can be interchangeably interpreted as either (a) the influence of WCA interactions or (b) the influence of the well section of the LJ potential. Subtracting the WCA contribution does not entirely exclude repulsion because the steepness of the LJ well at intermolecular separations close to σ indicates the onset of inter-particle repulsion regardless of the fact that $u(r_{ij})$ is negative. There is also the issue that the separation at which $u(r_{ij}) = 0$ does not match exactly, i.e., $r_{ij} = 2^{1/6}\sigma$ for the WCA potential compared with $r_{ij} = \sigma$ for the LJ potential. However, even with these caveats, Eq. (6) can reasonably be expected to isolate the different inter-particle influences that approximately correspond to the Barker-Henderson[7] separation of the LJ potential.

An alternative to these difference properties, would be to perform separate simulations for the WCA potential and an identified "attractive" part of the LJ potential. For example, Morsali *et al.*[26] have reported heat capacity calculations using potentials that are purely attractive and repulsive as originally proposed by Weeks *et al.*[8] However, the thermodynamic properties obtained from such an approach are arguably fictitious because no real fluid can exist with purely attractive interactions. Therefore, the difference values reported here provide a more realistic indication of the contribution from the different types of interaction.

A. Potential energy and pressure

Values of ΔU as functions of density and temperature are illustrated in Fig. 1. Figure 1(a) shows the results over the entire range of densities for different isotherms ($\varphi = 1.17$–2). It is apparent that, for all isotherms, ΔU decreases almost linearly with increasing density. More remarkably, the different isotherms are almost indistinguishable from each other, which clearly shows the dominance of the WCA potential in determining the potential energy of the fluid. Figure 1(b) shows the temperature dependence of ΔU at different isochores. For each isochore, ΔU increases with increasing temperature. However, the rate of increase is very small and as such ΔU is almost independent of temperature. This enables

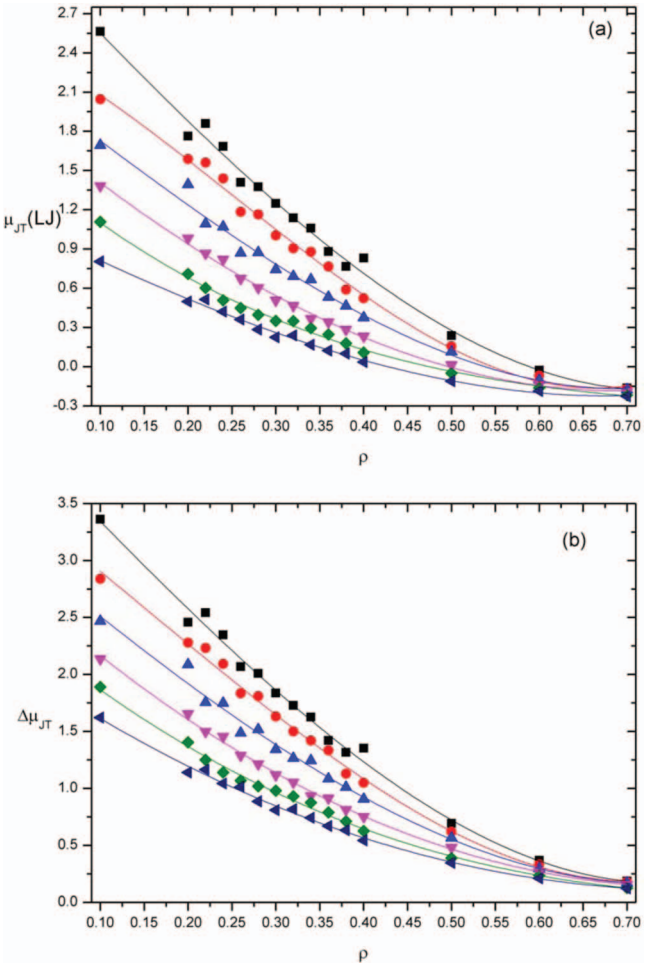

FIG. 9. (a) μ_{JT} for the LJ potential and (b) $\Delta\mu_{JT}$ as a function of density at different constant temperatures corresponding to $\varphi = 1.17$ (black ■), 1.25 (red ●), 1.4 (blue ▲), 1.6 (pink ▼), 1.8 (green ◆), and 2.0 (dark blue ◄). The solid lines are for guidance only.

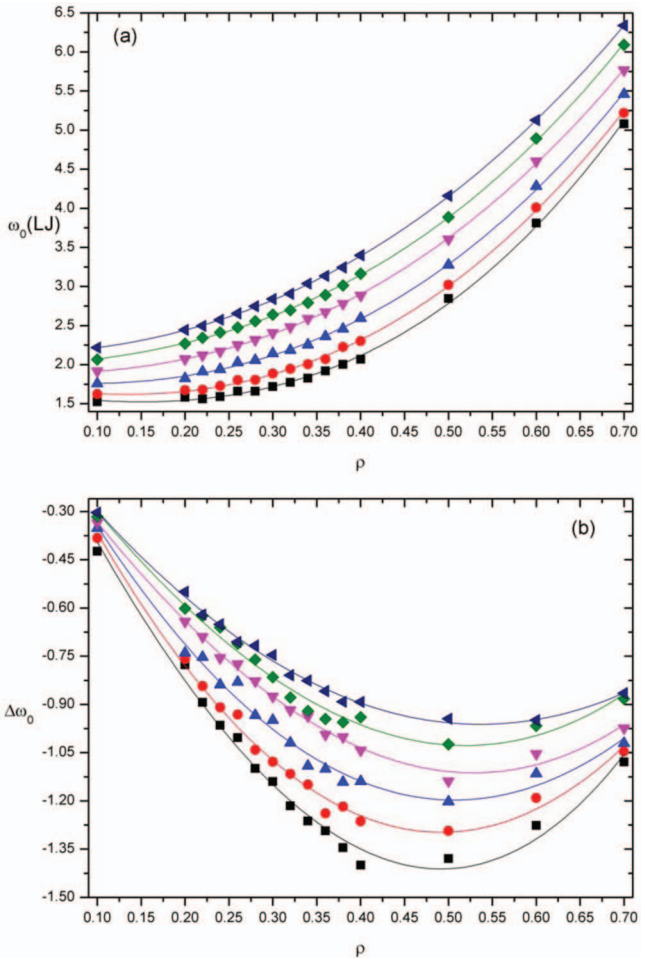

FIG. 11. (a) w_0 for the LJ potential and (b) Δw_0 as a function of density at different constant temperatures corresponding to $\varphi = 1.17$ (black ■), 1.25 (red ●), 1.4 (blue ▲), 1.6 (pink ▼), 1.8 (green ◆), and 2.0 (dark blue ◄). The solid lines are for guidance only.

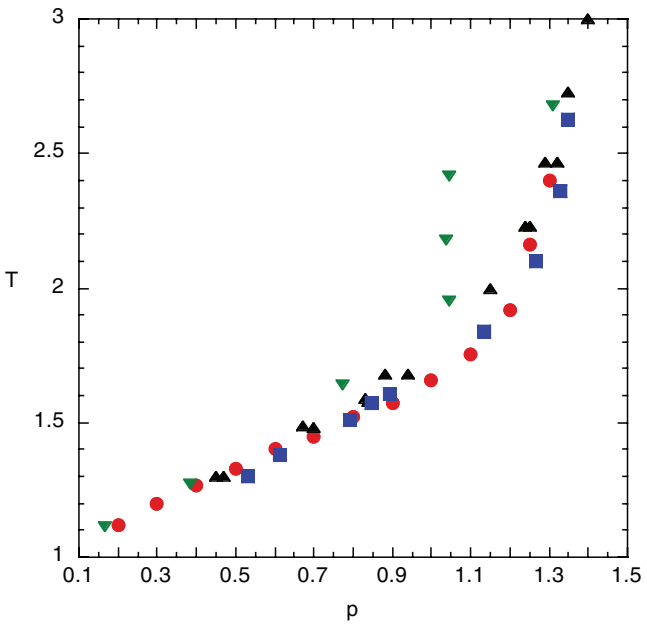

FIG. 10. Comparison of the Joule-Thomson inversion curve reported in this work (blue ■) with data reported from MC (red ●, Ref. 36) and MD (green ▼, Ref. 14 and black ▲, Ref. 39) simulations.

us to conclude that repulsive interactions are largely responsible for the temperature-dependence of U for the LJ fluid. For a real fluid, in the absence of repulsive interactions, the temperature dependence of E would arise mainly from the ideal gas term.

It is very well known that pressure is a continuous function of density and sensitive to the shape of the potential.[28] Values of both p_{LJ} and Δp as a function of density at different constant temperatures are illustrated in Fig. 2. It is apparent from Fig. 2(a) that the pressure isotherms for the LJ potential are shifted to higher pressures when the temperature is increased. In contrast, the values of Δp for the various isotherms are almost indistinguishable even at relatively high densities. Therefore, WCA repulsion dominates pressure at all densities.

Values of Δp as a function of temperature for different isochores are illustrated in Fig. 3. In the absence of the WCA contribution, the pressure of a LJ fluid is independent of temperature, depending only on density. This behavior is consistent with the near temperature-independent behavior of the potential energy (Fig. 1(b)). If the effect of inter-particle-repulsion were excluded from a real fluid, p would only be almost exclusively dependent on temperature via the ideal gas term.

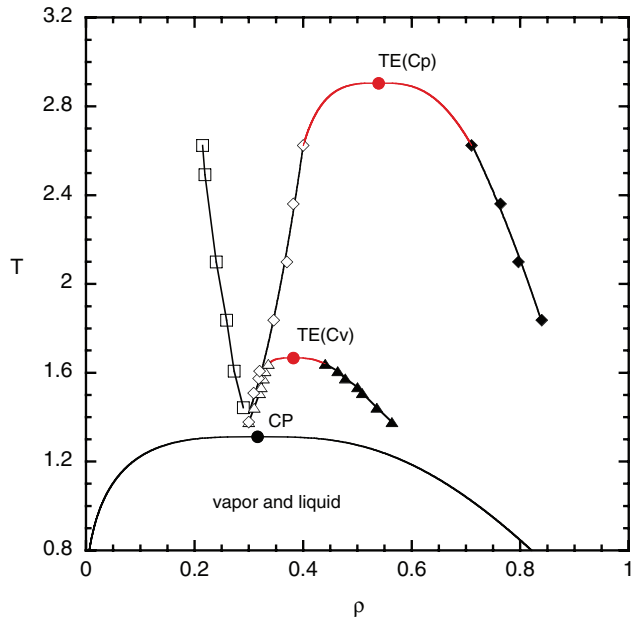

FIG. 12. Temperature-density behavior of the supercritical maxima (open symbols) and minima (closed symbols) of C_p(◇,◆), C_V(Δ, ▲), and α_T (□) for a Lennard-Jones fluid compared with its vapor-liquid coexistence curve (——, Ref. 46). The red lines linking the maxima and minima heat capacity data were obtained by fitting the data using the phase coexistence power relationship (Eq. (8)) with an exponent of $\beta = 0.32$. The vapor-liquid critical point (● CP, T = 1.312, $\rho = 0.316$, and $p = 0.128$, Ref. 27) and temperature extremes (red ● TE) for both C_V (T = 1.667, $\rho = 0.382$, and p = 0.384) and C_p (T = 2.905, $\rho = 0.539$, and p = 2.550) are identified.

Plačkov and Sadus[29] have previously identified the contribution of both r^{-12} and r^{-6} interactions to the pressure and energy for the vapor-liquid coexistence curve of the LJ potential. They concluded that the two contributions were of similar magnitude at sub-critical conditions. However, for the reasons discussed above, the current approach is likely to be a better alternative for accurately quantifying the relative influence of different types of particle interactions.

B. Isothermal and adiabatic compressibilities

The isothermal compressibility is positive in the one phase region. For an ordinary liquid, isothermal compressibility increases with temperature as it becomes less dense. Values of β_T calculated from the WCA potential are relatively small compared to the values from the LJ fluid. At high densities such as $\rho = 0.6$, the β_T value for the WCA potential is typically a third of the value obtained for the LJ potential. The relative difference between the WCA and LJ values increase with decreasing density. At low densities ($\rho < 0.3$), the value of β_T obtained from the LJ potential is often several times the WCA value. Similar trends are observed for β_S, although the difference in relative magnitudes is not as great.

Values of $\Delta\beta_S$ and $\Delta\beta_T$ as a function of density at different constant temperatures are illustrated in Fig. 4. As shown in Fig. 4(a), the adiabatic compressibility decreases monotonically with density in the low to mid density region ($\rho < 0.4$). A steady decrease in compressibility is observed for $\rho > 0.4$ and it approaches zero for $\rho > 0.6$ at all temperatures. A similar observation can be made for values of $\Delta\beta_T$ at values of $\varphi < 1.25$. However, at lower temperatures ($\varphi = 1.25$ and 1.17), there is a considerable increase in $\Delta\beta_T$, particularly at $\rho < 0.3$. It is well known[1] that the value of β_T diverges at the critical point ($\varphi = 1$, $\rho = 0.312$). Although both $\varphi = 1.25$ and 1.17 represent supercritical conditions, it is apparent that there is an influence from the critical point. The scatter of the data is similar to that experienced in the vicinity of the critical point due to finite size effects.[3]

The apparent maximum of β_T at $\varphi = 1.25$ and 1.17 is a manifestation of a well-known phenomenon[30] in which isotherms of derivative thermodynamic properties are observed to pass through a maximum in the supercritical phase. It is also observed for both isochoric and isobaric heat capacities and the thermal expansion coefficient. The locus of such maxima extends from above the critical temperature to a maximum supercritical temperature. In the vicinity of the critical point the different maxima lines merge into a single Widom line.[30] The origin of this phenomenon, which is also observed experimentally,[31] remains unresolved. It has been described[32] as a supercritical extension of the vapor pressure curve.

This phenomenon and the general behavior of both β_T and β_S are overwhelmingly governed by non-WCA interactions, i.e., interactions at intermolecular separations in the LJ potential well. It is of interest that the values of $\Delta\beta_S$ are much less influenced by the proximity to the critical point.

C. Thermal pressure coefficient

Values of γ_V for the LJ and WCA potentials as a function of temperature at different constant densities are illustrated in Fig. 5. The comparison indicates that values of γ_V obtained for the two potentials are almost identical at most temperatures or densities. Figure 5 also shows that for each isochore, γ_V for both potentials is almost constant with only a small negative gradient. It is only at low temperatures and higher densities that some differences are apparent. The close similarity of the values obtained for the two different potentials strongly indicates that γ_V depends only on the repulsive part of the potentials.

D. Thermal expansion coefficient

The thermal expansion coefficient is the measure of the tendency of matter to change volume in response to a change in temperature. At temperatures close to the critical point, the value of α_p diverges. The divergence of α_p is caused by its dependence on the isobaric heat capacity.

Values of $\Delta\alpha_p$ as a function of density at different constant temperatures are illustrated in Fig. 6. The values calculated from the LJ potential are higher than values calculated from the WCA potential, which means the $\Delta\alpha_p$ values depend mainly on the contribution from the LJ potential. At high temperatures ($\varphi = 2.0$, 1.8, and 1.6) a maximum is observed in the value of $\Delta\alpha_p$. Brazhkin *et al.*[32] estimated that there are α_p maxima at temperatures up to $\varphi = 2.8$. These maxima, become progressively more prominent as the temperature is further decreased ($\varphi = 1.4$, 1.25, and 1.17) toward the critical

temperature of the LJ fluid. The growing influence of the critical point is apparent in the scatter of the data, which indicates that finite size effects are important in the supercritical phase. This phenomenon can be attributed to interactions at interparticle separations in the well of the LJ potential because it occurs both in the presence and absence of WCA interactions.

E. Isochoric and isobaric heat capacities

Values of C_V for the LJ fluid at supercritical temperatures have been previously reported by Freasier *et al.*[33] from Monte Carlo simulations using the conventional fluctuation formula.[17,18] Our results for the LJ fluid are compared with these data in Fig. 7(a). At high temperatures ($T = 1.8$ and 1.6), there is good agreement between the two sets of data. At $T = 1.4$, the data are in agreement at most densities, except near the maximum in C_v. However at $T = 1.3$, we observe a much larger maximum in C_V. These differences can be largely attributed to the fact that Freasier *et al.*[33] truncated the LJ potential at a cut-off value of 2.5σ. Our calculations are for the full LJ potential with a cut-off distance of 6.5σ, which is considerably larger than 2.5σ. It is very well documented[34] that properties of fluids are sensitive to this, particularly in the vicinity of the critical point. At the lower temperatures, a minimum in C_V is also observed at a density of approximately $\rho = 0.6$.

A feature of the simulation results that is shared by real fluids is the observation of a maximum in C_V at supercritical temperatures. As discussed above, in the vicinity of the critical point the locus of these maxima form a so-called Widom line.[30] Hess *et al.*[35] have previously reported extensive C_V data for WCA particles and some LJ data have been reported recently.[16] For any given supercritical isotherm, values of C_V obtained from the WCA potential increase monotonically with increasing density. Our results for the WCA potential are in good agreement with these data. The absence of a maximum for the WCA potential indicates that this phenomenon can be attributed to interactions occurring at separations corresponding to the minimum of the LJ potential.

Isothermal values of ΔC_V as a function of density are illustrated in Fig. 7(b). The relatively small values of ΔC_V illustrate the dominance of WCA interactions in determining the magnitude of C_V. A peak in ΔC_V is observed for all isotherms but the phenomenon is much more pronounced at temperatures approaching the critical temperature ($\varphi = 1.17$ and 1.25). At these temperatures, there is a noticeable scatter in the data compared with higher temperatures ($\varphi = 1.6$, 1.8, and 2.0), which can be attributed to the influence of finite size effects.[35–37] Despite the dominance of WCA interactions in determining the overall magnitude of C_V, it is clear from this comparison that interactions associated with the well of the LJ potential are the controlling influence responsible for the C_V maxima.

Isothermal values of C_p for the LJ potential as a function of density are illustrated in Fig. 8(a). Most of the trends observed in C_p are the same as observed for C_V and the same conclusions can be applied. However, the WCA interactions have a relatively minor influence on the magnitude of C_p.

TABLE II. Absolute average values of various ratios of heat capacities (χ) for the LJ and WCA potentials at different temperatures and $0.1 \le \rho \le 0.7$.

	χ			
φ	$C_{p,WCA}/C_{p,LJ}$	$C_{p,WCA}/\Delta C_p$	$C_{V,WCA}/C_{V,LJ}$	$C_{V,WCA}/\Delta C_V$
1.17	0.31	0.54	0.86	7.57
1.25	0.39	0.72	0.89	9.59
1.40	0.49	1.03	0.93	13.94
1.60	0.57	1.43	0.95	20.56
1.80	0.64	1.89	0.97	29.84
2.00	0.69	2.29	0.97	37.32

This aspect can be clearly seen by comparing values of ΔC_p (Fig. 8(b)) to C_p (Fig. 8(a)). This means that the relative importance of contributions from WCA and LJ potential well interactions is reversed compared with their contributions to C_V.

To quantify the relative magnitudes of the contributions to C_V and C_p, for each isotherm we have calculated the absolute average (AA) of quantities "χ" as defined in Table II, i.e.,

$$AA = \frac{1}{N}\sum_{i=1}^{N} |\chi_i|, \tag{7}$$

where N is the total number of values of χ at different densities. The absolute averages of heat capacity ratios calculated using Eq. (7) are given in Table II.

The AAs of the $C_{p,V,WCA}/C_{p,V,LJ}$ ratios increase with temperature, which implies that $C_{p,V,WCA}$ increases faster than $C_{p,V,LJ}$ and that the contribution of the LJ-well is higher at lower temperatures. The AA of the $C_{V,WCA}/C_{V,LJ}$ ratios is close to unity in most cases, which implies that the $C_{V,WCA}$ values are comparable to $C_{V,LJ}$ for each isochore. This is further illustrated by the very high values for the $C_{V,WCA}/\Delta C_V$, ratio which has a value greater than 37 at a temperature twice the critical temperature of the LJ fluid. The $C_{V,LJ}$ values are very small compared with $C_{V,WCA}$.

The AAs for the $C_{p,WCA}/\Delta C_p$ ratio also increase with temperature, however the increase is small compared with that of $C_{V,WCA}/\Delta C_V$ ratios. These small AA values highlight that $C_{p,WCA}$ is very small compared to $C_{p,LJ}$ values calculated from the LJ potential. The contribution of the LJ-well dominates the magnitude of C_p. For both C_V and C_p, the reduction of the maxima with increasing temperature also coincides with an increasing contribution of WCA interactions relative to the LJ potential well.

F. Joule-Thomson coefficient

Values of μ_{JT} for the LJ potential and $\Delta\mu_{JT}$ are illustrated in Fig. 9 as functions of density at different constant temperatures. As shown in Fig. 9(a), μ_{JT} for the LJ fluid decreases with density along the isotherm, with some fluctuations near the critical point, attaining a negative value at higher densities. This means that there is an inversion curve (i.e., locus of $\mu_{JT} = 0$) for the LJ fluid. There are two temperatures at which $\mu_{JT} = 0$: the first one is in the lower density supercritical fluid part of the phase diagram and the other point[39] is when the

fluid approaches the liquid state as $p \rightarrow 0$. In the region where $\mu_{JT} > 0$ for the LJ fluid ($0.1 \leq \rho \leq 0.6$), the decrease in pressure has caused a decrease in temperature which occurs as a result of lower initial pressure. In the region where $\mu_{JT} > 0$ ($\rho \geq 0.6$ for the LJ potential and at all densities for the WCA potential), the decrease in pressure causes an increase in temperature, i.e., there will be heating on expansion. The values of μ_{JT} from the WCA are negative at all temperatures and densities, which is reflected in the larger values of $\Delta\mu_{JT}$ (Fig. 9(b)) compared with μ_{JT} for the LJ potential (Fig. 9(a)). An important consequence of the negative contribution from WCA interactions is that it makes an inversion curve possible for the LJ potential.

It should be noted that obtaining the inversion curve is a challenge for both experimental methods and molecular simulation. The most extensive calculations of the inversion curve for the LJ fluid have been reported[37,38] from MC simulations. Escobedo and Chen[14] reported good results using a MC multi-histogram re-weighing technique. In contrast, as shown in Fig. 10, Heyes and Llaguno[39] reported considerable difficulties in accurately locating the inversion curve from conventional MD simulation. Kioupis *et al.*[40,41] addressed this problem via a specialised constant enthalpy MD algorithm.

To obtain the inversion curve, we first calculated the density at which μ_{JT} is zero for each of the isotherms in Fig. 9(a). A change in sign takes place when the density is between 0.6 and 1.0. We then found the corresponding value of the pressure at that density from Fig. 2(a) for each of the isotherms. This was achieved by finding the best fit to each of the isotherms and then using a fitting equation to calculate the pressure at each of the densities where $\mu_{JT} = 0$. This only results in a partial inversion curve because, as shown in Refs. 42–44, a very large number of simulation results at $\varphi \geq 4.5$ would be required to obtain the complete inversion curve. The coordinates for the LJ inversion curve extrapolated in this way from our simulations are given in Table III and a comparison with literature values is given in Fig. 10.

The comparison in Fig. 10 indicates that our inversion temperature is in good agreement with the data of Colina and Müller[37] and Kioupis *et al.*,[41] which are consistent with calculations obtained from a LJ equation of state.[45] We did not observe the difficulties reported by Heyes and Llaguno,[39] which suggests that the $NVE\vec{P}\vec{G}$ MD ensemble is particularly beneficial for this property. As noted above, the inversion curve is difficult to calculate accurately. Escobedo and Chen[14] identified factors such as insufficient cycles to accumulate simulation averages, system size, and cut-off values as possible sources of discrepancies. Our system size of 2000 is larger than the 256 (Ref. 14) or 500 (Refs. 14 and 37) particle simulations reported previously; a large cut-off value was used; and the averages were accumulated for the equivalent of 2×10^6 MC cycles compared with 10^4 (Ref. 37) and 10^5 (Ref. 14) cycles used elsewhere.

TABLE III. Coordinates of the partial Joule-Thomson inversion curve for the Lennard-Jones fluid.

φ	1.0	1.05	1.15	1.2	1.225	1.40	1.60	1.80	2.0
p	0.530	0.615	0.794	0.847	0.894	1.134	1.266	1.329	1.348
ρ	0.637	0.617	0.595	0.589	0.582	0.553	0.510	0.469	0.424

G. Speed of sound

Values of ω_0 calculated for the LJ fluid and $\Delta\omega_0$ are illustrated in Fig. 11 as a function of density at different constant temperatures. As shown in Fig. 11(a), ω_0 increases with density along each isotherm without any noticeable fluctuations near the critical point. The speed of sound approaches a minimum value near the critical point. The power law expression for ω_0 at the critical point predicts the speed of sound to be zero.[1]

The pressure calculated from the WCA potential is higher than the value calculated from the LJ potential (Fig. 2(b)). The speed of sound depends on pressure (see Table I), which means that values of ω_0 for the WCA potential will be higher than that from the LJ potential. The large contribution of WCA interactions is evident from the values of $\Delta\omega_0$ in Fig. 11(b). In the absence of the WCA contribution, ω_0 would have physically unrealistic negative values. This highlights the important role of repulsion, particularly at small separations, on the thermodynamic properties of fluids.

H. Maxima and minima of thermodynamic properties

We have observed that α_p, C_V, and C_p obtained for a Lennard-Jones fluid have distinct maxima in the supercritical phase, which is entirely consistent with the behavior of real fluids. We have also found that both C_V and C_p have minima at high densities. To the best of our knowledge C_p minima have not been reported previously for the Lennard-Jones fluid. The loci of both maxima and minima for the thermodynamic properties are illustrated in Fig. 12 in conjunction with the vapor-liquid phase diagram for a Lennard-Jones fluid.[27,46] It should be noted that there is a degree of scatter in the simulation data, particularly in the vicinity of the maxima, which means that the coordinates should be treated as approximations only.

As temperature is increased, Fig. 12 shows that the locus of α_p maxima veers progressively to densities that are much less that the critical density ($\rho = 0.316$, Ref. 27). In common with the maxima of all thermodynamic quantities, it becomes less pronounced with increasing temperature and disappears at an undetermined temperature beyond $T = 2.624$. This behavior is consistent with other work in the literature[32] for the Lennard-Jones fluid.

The behavior of the maxima and minima of C_V and C_p are particularly noteworthy. At all supercritical temperatures, both a maxima and minima were observed for C_V. It is apparent from Fig. 12 that the C_V maxima initially occurs at a density close to the critical density but progressively shifts to higher densities. In contrast, the C_V minima commences from a relatively high density and progressively shifts to lower densities, that is, the loci of C_V maxima and C_V minima are apparently converging to a common point or a shared temperature extreme (T_E) after which no further maxima or minima are observed. We find that the maxima and minima loci can be

fitted to the same power law as vapor-liquid equilibria and the densities are consistent with the law of rectilinear diameters,[47] i.e.,

$$\left.\begin{aligned}\rho_{\min}-\rho_{\max} &= A\left|1-\frac{T}{T_E}\right|^{\beta}\\ \frac{(\rho_{\min}+\rho_{\max})}{2} &= \rho_E + C(T_E - T)\end{aligned}\right\}, \tag{8}$$

where A and C are constants. Using a value of $\beta = 0.32$, we find that $T_{E,C_V} = 1.667$, $\rho_{E,C_V} = 0.382$, and $p_{E,C_V} = 0.384$, where p_{E,C_V} was obtained from an independent simulation at conditions corresponding to T_{E,C_V} and ρ_{E,C_V}.

Experimental measurements for the isochoric heat capacity at supercritical temperatures have been reported,[48] which exhibit both maxima and minima curves that converge at a common point. Experimental heat capacity data[49] for diethyl ether provide a recent example of both maxima and minima behavior. The phenomena observed for the Lennard-Jones fluid are qualitatively similar except that the minima curve for diethyl ether first veers to lower densities before connecting to the maxima curve at a density slightly above the critical density.

At temperatures immediately above the critical point, only maxima in C_p are observed initially. It is evident from Fig. 12 that the densities of the maxima of C_p and C_V largely coincide. However, at temperatures above $T_{E,C_V} = 1.657$, minima are also observed for C_p. The C_p minima curve commences at much higher densities than the corresponding C_V curve. The position of the C_p minima shifts to lower densities with increasing temperatures whereas the C_p maxima is located at progressively higher densities, which indicates that the convergence of the two curves is likely. It is apparent from Fig. 12 that the C_p phenomena occur over a much larger range of both density and temperature than for C_V. Equation (8) can also be used to locate the coordinates of the temperature extreme, which is found at $T_{E,C_p} = 2.905$, $\rho_{E,C_p} = 0.539$, and $p_{E,C_p} = 2.550$.

For a given isotherm, maxima in either C_V or C_p correspond to

$$\left.\begin{aligned}\left(\frac{\partial C_{p,V}}{\partial V}\right)_{T<T_E>T_c} &= 0\\ \left(\frac{\partial^2 C_{p,V}}{\partial V^2}\right)_{T<T_E>T_c} &< 0\end{aligned}\right\} \tag{9}$$

whereas, the occurrence of minima on the isotherm means

$$\left.\begin{aligned}\left(\frac{\partial C_{p,V}}{\partial V}\right)_{T<T_E>T_c} &= 0\\ \left(\frac{\partial^2 C_{p,V}}{\partial V^2}\right)_{T<T_E>T_c} &> 0\end{aligned}\right\}. \tag{10}$$

The convergence of the maxima and minima curves to a common point suggests that this is a point of inflection characterized by

$$\left.\begin{aligned}\left(\frac{\partial C_{p,V}}{\partial V}\right)_{T=T_E} &= 0\\ \left(\frac{\partial^2 C_{p,V}}{\partial V^2}\right)_{T=T_E} &= 0\\ \left(\frac{\partial^3 C_{p,V}}{\partial V^3}\right)_{T=T_E} &\neq 0\end{aligned}\right\}. \tag{11}$$

The critical isotherm of a pure fluid also exhibits an inflection point in its pressure-volume behavior. The behavior of heat capacity in the supercritical region appears analogous to the behavior of pressure at sub-critical isotherms. Experimental values of pressure are constant along all sub-critical isotherms within the two-phase region bounded by the coexisting liquid and vapor densities whereas there is a steep pressure gradient on either side of the coexistence curve. Similarly, there is a noticeable heat capacity gradient at densities outside of the region bounded by the maxima and minima densities. Isotherms above the critical point display a smooth variation in pressure at all densities and similar behavior is observed for heat capacities for isotherms with $T > T_E$.

Previous calculations in the literature[32] for the Lennard-Jones potential indicate that the C_p maxima, which initially trends towards increasing densities, diverges back to the critical density at high temperatures. To the best of our knowledge, the existence of C_p minima have not been previously observed either in the Lennard-Jones fluid or real fluids. This is in contrast with experimental evidence[48,49] for the existence of such behavior in C_V. The magnitude of the minima is much less pronounced than the maxima and it diminishes with increasing temperatures. This means that it could be easily overlooked, particularly if the density increments are not sufficiently small. The maxima also diminish with increasing temperature and become more difficult to detect at high temperatures. Heat capacity measurements in the supercritical phase are focused primarily in the region of the maxima, which is often well outside of the region in which minima are likely to be located. The preference for performing measurements at constant pressure also means that densities corresponding to the minima may not be encountered routinely.

The existence of a locus of minima provides a mechanism for the hitherto largely unexplained termination of the locus of maxima. The locus of maxima is sometimes interpreted[50] as a demarcation point between "gas-like" and "liquid-like" behavior in the supercritical phase. Assuming that such a description is valid, then the locus of minima could be logically interpreted as a second demarcation line.

IV. CONCLUSIONS

The $NVE\vec{P}\vec{G}$ MD ensemble can be used to directly obtain all of the thermodynamic properties of supercritical fluids. The comparison of results obtained for the LJ and WCA potentials provides insights into the contribution of intermolecular interaction on thermodynamic properties. An important insight arising from this work is that the role of WCA and LJ potential well interactions are different depending on the thermodynamic property. The complexity of the

thermodynamic properties in terms of the phase-space functions means that only general observations can be safely made linking thermodynamic properties to specific interactions.

The temperature dependence of U can be largely attributed to repulsive WCA interactions and in the absence of such interactions the temperature-dependence of p would be almost entirely due to the ideal gas term. The contributions of WCA interactions ensure that the LJ potential has a μ_{JT} inversion curve, which has been partially determined in this work. They also ensure that physically realistic values are obtained for w_0.

Repulsive interactions have an important role in β_T, whereas their contribution to β_S is small. The values of γ_V obtained for either the WCA or LJ potentials are almost identical for a large range of both temperatures and densities. Repulsion has only a small influence of values of $\Delta\alpha_p$, which pass through a maximum value at supercritical temperatures in the proximity of the critical point. This behavior is also a characteristic of C_V and C_p and in both cases it is apparent that it is determined by interactions at separations within the LJ potential well. The contribution of repulsive interactions dominates the magnitude of C_V, whereas the attractive part of the potential is the largest contributor to C_p. In general, we observe that much of the divergent behavior of α_p, β_T, C_V, and C_p occurs at nearest neighbor separations close to values corresponding to the minimum of the LJ potential well and as such the influence of WCA interactions is minimal.

At supercritical temperatures, both maxima and minima values of C_V and C_p are observed for the Lennard-Jones fluid. Supercritical C_V and C_p maxima and C_V minima are well documented from experimental studies of real fluids. In contrast, the existence of a locus of C_p minima has not been observed previously. The maxima and minima loci for both C_V and C_p appear to converge to a common point. We postulate that the temperature-density behavior of these curves obey the same power law as the coexistence curve with an exponent of $\beta = 0.32$. The convergence of the two branches of the C_p curves provides an alternative explanation for the terminating value of the C_p maxima in supercritical fluids.

ACKNOWLEDGMENTS

We thank the National Computing Infrastructure (NCI) for an allocation of computing time. One of us (T.M.Y.) thanks Swinburne University of Technology for a postgraduate research award.

[1]C. G. Gray and K. E. Gubbins, *Theory of Molecular Fluids Vol. 1: Fundamentals* (Clarendon Press, Oxford, 1984); J.-P. Hansen and I. R. McDonald, *Theory of Simple Liquids*, 2nd ed. (Academic Press, London, 1986).
[2]Y. S. Wei and R. J. Sadus, AIChE J. **46**, 169 (2000).
[3]R. J. Sadus, *Molecular Simulation of Fluids: Theory, Algorithms and Object-Orientation* (Elsevier, Amsterdam, 1999).
[4]A. Ahmed and R. J. Sadus, J. Chem. Phys. **131**, 174504 (2009).
[5]A. Z. Panagiotopoulos, Mol. Phys. **61**, 813 (1987); R. J. Sadus and J. M. Prausnitz, J. Chem. Phys. **104**, 4784 (1996).
[6]D. A. McQuarrie and J. L. Katz, J. Chem. Phys. **44**, 2393 (1966).
[7]J. A. Barker and D. Henderson, J. Chem. Phys. **47**, 4714 (1967).
[8]J. D. Weeks, D. Chandler, and H. C. Andersen, J. Chem. Phys. **54**, 5237 (1971).
[9]M. Kröger, Phys. Rep. **390**, 453 (2004).
[10]J. T. Bosko, B. D. Todd, and R. J. Sadus, J. Chem. Phys. **124**, 044910 (2006).
[11]A. Ahmed and R. J. Sadus, Phys. Rev. E **80**, 061101 (2009).
[12]F. W. de Wette, L. H. Fowler, and B. R. A. Nijboer, Physica **54**, 292 (1971); A. Toro-Labbé, R. Lustig, and W. A. Steele, Mol. Phys. **67**, 1385 (1989): D. Boda, T. Lukács, J. Liszi, and I. Szalai, Fluid Phase Equilib. **119**, 1 (1996); J. J. Nicolas, K. E. Gubbins, W. B. Streett, and D. J. Tildesley, Mol. Phys. **37**, 1429 (1979); F. Cuadros, A. Mulero, and W. Ahumada, Thermochim. Acta **277**, 85 (1996); F. Cuadros and W. Ahumada, *ibid.* **297**, 109 (1997); F. Cuadros, A. Mulero, and C. A. Faúndez, Mol. Phys. **98**, 899 (2000); V. G. Baidokov, S. P. Protsenko, and Z. R. Kozlova, Chem. Phys. Lett. **447**, 236 (2007).
[13]R. Lustig, A. Toro-Labbé, and W. A. Steele, Fluid Phase Equilib. **48**, 1 (1989).
[14]F. A. Escobedo and Z. Chen, Mol. Simul. **26**, 395 (2001).
[15]G. Galliero and C. Boned, J. Chem. Phys. **129**, 074506 (2008).
[16]H.-O. May and P. Mausbach, Phys. Rev. E **85**, 031201 (2012).
[17]J. L. Lebowitz, J. K. Percus, and L. Verlet, Phys. Rev. **153**, 250 (1967).
[18]P. S. Y. Cheung, Mol. Phys. **33**, 519 (1977).
[19]R. Lustig, J. Chem. Phys. **100**, 3048 (1994).
[20]R. Lustig, J. Chem. Phys. **100**, 3060 (1994).
[21]R. Lustig, J. Chem. Phys. **100**, 3068 (1994).
[22]R. Lustig, J. Chem. Phys. **109**, 8816 (1998).
[23]L. Pártay and P. Jedlovszky, J. Phys. Chem. **123**, 024502 (2005); M. Bernabei, A. Botti, F. Bruni, M. A. Ricci, and K. Soper, Phys. Rev. E **78**, 021505 (2008); M. Bernabei and M. A. Ricci, J. Phys.: Condens. Matter **20**, 494208 (2008).
[24]K. Meier and S. Kabelac, J. Chem. Phys. **124**, 064104 (2006).
[25]P. Mausbach and R. J. Sadus, J. Chem. Phys. **134**, 114515 (2011).
[26]A. Morsali, S. A. Beyramabadi, S. H. Vahidi, and M. Ghorbani, Mol. Phys. **110**, 483 (2012).
[27]J. J. Potoff and A. Z. Panagiotopoulos, J. Chem. Phys. **109**, 10914 (1998).
[28]P. S. Vogt, R. Liapine, B. Kirchner, A. J. Dyson, H. Huber, G. Marcelli, and R. J. Sadus, Phys. Chem. Chem. Phys. **3**, 1297 (2001).
[29]Đ. Plačkov and R. J. Sadus, Fluid Phase Equilib. **134**, 77 (1997).
[30]L. Xu, P. Kumar, S. V. Buldyrev, S.-H. Chen, P. H. Poole, F. Sciortino, and H. E. Stanley, Proc. Natl. Acad. Sci. U.S.A. **102**, 16558 (2005).
[31]*Heat Capacities: Liquids, Solutions and Vapours*, edited by E. Wilhelm and T. Letcher (The Royal Society of Chemistry, Cambridge, 2010).
[32]V. V. Brazhkin, Y. D. Fomin, A. G. Lyapin, V. N. Ryzhov, and E. N. Tsiok, J. Phys. Chem. B **115**, 14112 (2011).
[33]B. C. Freasier, A. Czezowski, and R. J. Bearman, J. Chem. Phys. **101**, 7934 (1994).
[34]W. Shi and J. K. Johnson, Fluid Phase Equilib. **187–188**, 171 (2001).
[35]S. Hess, M. Kröger, and H. Voigt, Physica A **250**, 58 (1998).
[36]B. C. Freasier, C. E. Woodward, and R. J. Bearman, J. Chem. Phys. **105**, 3686 (1996).
[37]C. Colina and E. A. Müller, Mol. Simul. **19**, 237 (1997).
[38]C. M. Colina and E. A. Müller, Int. J. Thermophys. **20**, 229 (1999).
[39]D. M. Heyes and C. T. Llaguno, Chem. Phys. **168**, 61 (1992).
[40]L. I. Kioupis and E. J. Maginn, Fluid Phase Equilib. **200**, 75 (2002).
[41]L. I. Kioupis, G. Arya, and E. J. Maginn, Fluid Phase Equilib. **200**, 93 (2002).
[42]Y. Song and E. A. Mason, J. Chem. Phys. **91**, 7840 (1989).
[43]J. Kolafa and I. Nezbeda, Fluid Phase Equilib. **100**, 1 (1994).
[44]W. W. Wood and F. R. Parker, J. Chem. Phys. **27**, 720 (1957).
[45]J. K. Johnson, J. A. Zollweg, and K. E. Gubbins, Mol. Phys. **78**, 591 (1993).
[46]D. Kofke, J. Chem. Phys. **98**, 4149 (1993).
[47]R. J. Sadus, Mol. Phys. **87**, 979 (1996).
[48]A. I. Abdulagatov, G. V. Stepanov, I. M. Abdulagatov, A. E. Ramaznova, and G. S. Alidultanova, Chem. Eng. Commun. **190**, 1499 (2003).
[49]N. G. Polikhronidi, I. M. Abdulagotov, R. G. Butyrova, G. V. Stepanov, J. T. Wu, and E. E. Ustuzhanin, Int. J. Thermophys. **33**, 185 (2012).
[50]G. G. Simeoni, T. Bryk, F. A. Gorelli, M. Krisch, G. Ruocco, M. Santoro, and T. Scopigno, Nat. Phys. **6**, 503 (2010).